CHARACTERIZATION OF SELECTIVE LASER MELTING 3D-PRINTED Ti64 ALLOY

Trinh Van Trung*, Nguyen Anh Son, Le Thai Hung, Hoang Van Vuong, Nguyen Minh Thuyet
School of Materials Science and Engineering - Hanoi University of Science and Technology

ARTICLE INFO

Received: 01/3/2025
Revised: 09/5/2025
Published: 09/5/2025

KEYWORDS

Ti64 alloy
3D printing technology
Selective laser melting
Porous defect
Mechanical properties

ABSTRACT

Tensile testing Ti64 alloy samples were 3D printed using SLM (Selective Laser Melting) technology. The main printing parameters were as follows: a laser spot diameter of 180 µm, a hatch spacing of 140 µm, a scanning speed of 1600 mm/s, a laser power of 380 W, a layer thickness of 45 µm, and a continuous printing strategy with alternating layer angles of 45°. The microstructure of the printed sample has a significant influence on its properties. Hence, this study aims to investigate the microstructure and properties of 3D-printed Ti64 alloy objects produced using SLM technology. Various analytical techniques and equipment were used to study the surface morphology, fracture surface, microstructure, and hardness of the 3D-printed Ti64 alloy samples, including an optical microscope, digital optical microscope, X-ray diffraction, scanning electron microscope with an EDS probe, and HV hardness tester. The results indicate that the printed sample primarily consists of the α/α' phase, with an average hardness of approximately 343 HV, an elastic modulus of 24.34 GPa, a yield strength of 93.5 MPa, an ultimate tensile strength of 1049.4 MPa, and an elongation of 12.8%. The printed sample's surface exhibits high roughness and contains numerous porous defects, and mechanical properties that are inferior to those of conventionally manufactured Ti64 alloy.

ĐẶC TÍNH CỦA HỢP KIM Ti64 IN 3D BẰNG CÔNG NGHỆ NUNG CHẢY LAZE CHỌN LỌC

Trịnh Văn Trung*, Nguyễn Anh Sơn, Lê Thái Hùng, Hoàng Văn Vương, Nguyễn Minh Thuyết
Trường Vật liệu - Đại học Bách khoa Hà Nội

THÔNG TIN BÀI BÁO

Ngày nhận bài: 01/3/2025
Ngày hoàn thiện: 09/5/2025
Ngày đăng: 09/5/2025

TỪ KHÓA

Hợp kim Ti64
Công nghệ in 3D
Nung chảy laze chọn lọc
Khuyết tật xốp
Tính chất cơ học

TÓM TẮT

Các mẫu hợp kim Ti64 thử nghiệm kéo được in 3D bằng công nghệ nung chảy laze chọn lọc SLM (Selective Laser Melting) với các thông số chính của quy trình in gồm đường kính điểm laser (180 µm), khoảng cách giữa các đường in (140 µm), tốc độ quét (1600 mm/giây), công suất laser (380 W), độ dày lớp in (45 µm) và góc in giữa 2 lớp in liên tiếp (45^o). Cấu trúc vi mô của mẫu in có ảnh hưởng lớn đến các tính chất của nó. Do vậy, nghiên cứu này nhằm mục đích khảo sát cấu trúc vi mô và cơ tính của hợp kim Ti64 in 3D được tạo ra bằng công nghệ in SLM. Các thiết bị và phương pháp phân tích như kính hiển vi quang học, kính hiển vi quang học kỹ thuật số, nhiễu xạ tia X, kính hiển vi điện tử quét có đầu dò EDS và thiết bị đo độ cứng HV đã được sử dụng để nghiên cứu hình thái bề mặt và bề mặt gãy của các mẫu in, cấu trúc vi mô, tổ chức pha và độ cứng của các mẫu hợp kim Ti64 in 3D. Kết quả cho thấy mẫu in có tổ chức pha chủ yếu là α/α', độ cứng trung bình khoảng 343 HV, mô đun đàn hồi bằng 24,34 GPa; giới hạn chảy bằng 93,5 MPa, giới hạn bền bằng 1049,4 MPa và giới hạn dẻo bằng 12,8%. Bề mặt mẫu in có độ nhám cao, vật in vẫn còn nhiều khuyết tật xốp và tính chất cơ học của mẫu in không cao bằng mẫu hợp kim truyền thống.

DOI: https://doi.org/10.34238/tnu-jst.12165

* Corresponding author. *Email: trung.trinhvan@hust.edu.vn*

1. Introduction

Ti64, or Ti6Al4V, is a titanium alloy known for its high fatigue and creep resistance, high specific strength, good corrosion resistance, and excellent biocompatibility, among other properties. As a result, it is commonly used in fields such as mechanical engineering, aeronautics, aerospace, and biomedical device manufacturing. In its equilibrium state, this type of titanium alloy consists of two phases: α and β. The aluminum element stabilizes the α phase and expands the α region on the phase diagram of titanium alloys. In contrast, vanadium stabilizes the β phase and expands the β region [1] – [3].

3D printing technology has garnered significant attention from scientists and engineers due to its ability to create rapid prototypes and models with complex shapes and structures while minimizing material waste [4]. This technology involves depositing each layer of material in a precise manner with the assistance of software based on detailed design models of an object [5] –[7].

The application of 3D printing technology to the production of Ti64 alloy products has been widely researched and implemented. The structure, microstructure, and properties of printed objects depend on several factors, such as the printing technology (electron beam-based powder bed fusion, laser-based powder bed fusion, or directed energy deposition), printing parameters, and processing conditions [6] – [8]. However, when 3D printing is used for metal materials in general and Ti64 alloy in particular, it often results in objects, parts, or products with various defects, such as pores, anisotropic structures, and mechanical properties or durability that are inferior to those of conventionally manufactured products [6] – [11]. The hardness of both 3D-printed Ti6Al4V samples produced by LBM and EBM was similar and slightly higher than that of cast and wrought alloys [12]. The increased hardness of the Ti6Al4V sample is attributed to the formation of the martensite phase during rapid cooling in the 3D printing process [13]. While pores and other defects cannot be completely eliminated, they should be minimized [14]. This is because when defects such as pores and lack of fusion are present in large amounts, fatigue performance tends to deteriorate, and cracks may initiate either within the bulk material or at the surface [15]. Hence, the microstructure of the printed sample significantly influences its properties. Therefore, this study aims to investigate the microstructure and properties of Ti64 alloy objects produced via Selective Laser Melting (SLM) 3D-printing technology.

2. Experimental procedure

The chemical composition and particle size distribution of the Ti64 printing powder used in this study are shown in Table 1 and Table 2. The chemical composition of the printing powder corresponds to the Ti6Al4V alloy (Grade 23). Laser diffraction and Sieve analysis methods were used for the analysis of particle size distribution of the Ti64 printing powder according to ASTM-B822 / B821 and ASTM B214 standards, respectively. The spherical printing powder particles have a size range that meets all specification requirements.

Table 1. *Chemical composition of 3D-printed power.*

Chemical composition	Al	V	Fe	Y	C	O	N	H	Ti
Standard	6.00 - 6.50	3.80 - 4.50	< 0.25	< 0.005	< 0.05	< 0.12	< 0.03	< 0.012	Bal.
Ti64 sample	6.28	3.97	0.15	< 0.005	< 0.005	0.085	0.008	0.004	Bal.

Selective Laser Melting (SLM) technology was used to print Ti64 samples in the form of tensile testing specimens, as shown in Figure 1. The printing was carried out using a Concept Laser (M2 - Series 5) device with the following technological parameters: a laser spot diameter of 180 μm, a hatch spacing of 140 μm, a scanning speed of 1600 mm/s, a laser power of 380 W, a layer thickness of 45 μm, and a continuous printing strategy with a layering angle of 45° between two consecutive layers. After printing, the sample cooled with the environment in the printing chamber.

Table 2. *Particle size distribution*

Analysis	Specification requirements			Results, µm	Meets Specification
Laser Diffraction ASTM-B822 / B821	**Vol. %**	**Min, µm**	**Max, µm**		
	D10	15	-	15	Yes
	D90	-	50	44	Yes
Sieve Analysis ASTM B214	**Size, µm**	**Min, wt. %**	**Max, wt. %**	**Results, wt. %**	**Meets Specification**
	+45	-	5	3.3	Yes
	-45	95	-	96.7	Yes

Figure 1. *Image of the 3D printed Ti64 alloy tensile testing sample*

Tensile test specimens (according to ASTM E8) were evaluated for mechanical properties using the MTS E45.105 multi-purpose tensile testing device. The as-received tensile test specimen was sliced along a plane perpendicular to the tensile test specimen axis into disc-shaped samples approximately 5 mm thick for microstructure examination and hardness measurement. Hardness was measured at three different positions on the cut sample surface, and the average value was calculated.

The surface morphology of the printed samples, the fracture surfaces of the tensile test specimens, and the microstructure and hardness of the 3D-printed Ti64 alloy samples were examined using an optical microscope (Olympus GX53), a digital optical microscope (Keyence VHX-7000), X-ray diffraction (Panalytical AERIS), a scanning electron microscope with an EDS probe (JEOL JSM-IT200), and an HV hardness tester (Qualitest Qualirock-RS).

3. Results and Discussion

3.1. Surface roughness and chemical composition

Figure 2 presents an image of the tensile test specimen's surface at gage length region captured using a VHX-7000 digital microscope. The average roughness was measured at three different positions, revealing a significantly rough printed surface with an Ra value of 72.87 µm.

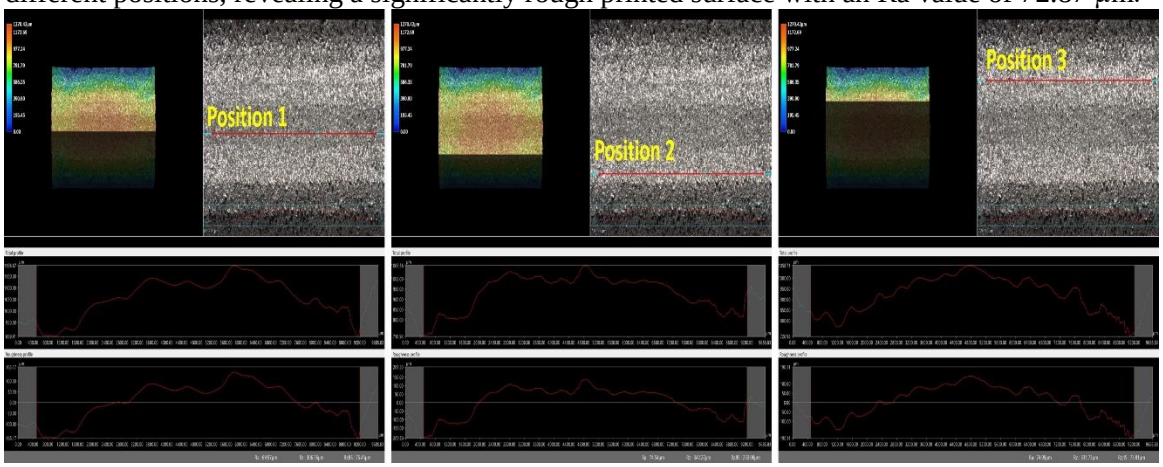

Figure 2. *Roughness analysis on printed sample surface*

High surface roughness is a characteristic of 3D printing technology in general and metal 3D printing in particular. This roughness is primarily due to the presence of unmelted powder

particles on the surface of metal 3D-printed objects, as shown in Figure 3a. As a result, additional surface finishing steps are often required to enhance the smoothness of 3D-printed components [6]. Additionally, EDS analysis results (Figure 3b) indicate that the printed sample is primarily composed of Ti, Al, and V—elements characteristic of the Ti-6Al-4V alloy.

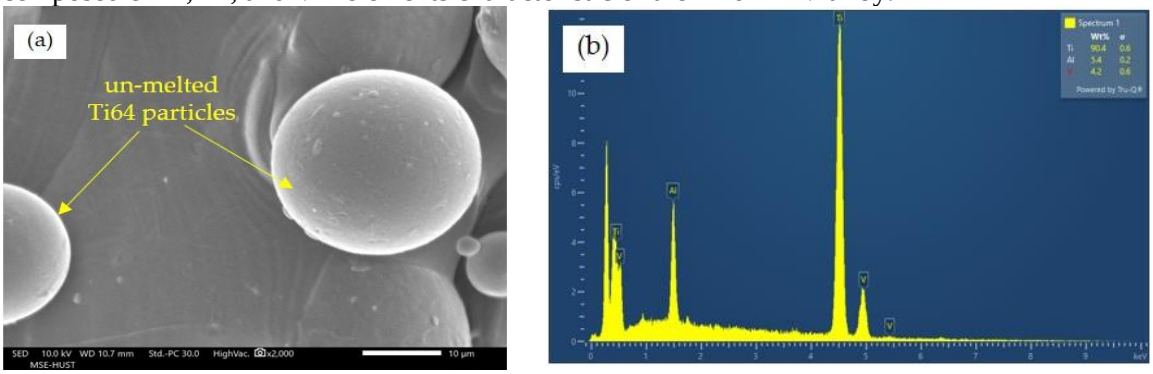

Figure 3. *a) SEM image and b) analysis result by energy dispersive spectroscopy (EDS) on the printed sample surface*

3.2. Microstructure

The microstructure of the Ti64 alloy sample is shown in Figure 4. Analysis results indicate that the surface of the printed sample exhibits multiple printed lines interwoven at a 45° angle (Figure 4a). Additionally, the results in Figures 4 show that there are many pores. The structure of the printed sample is anisotropic (Figure 4a). The dark, needle-like structures observed in Figure 4b represent the martensitic phase of the titanium alloy. The formation of this martensitic phase in 3D-printed objects is attributed to the rapid cooling rate characteristic of Selective Laser Melting (SLM) in metal 3D printing technology [6], [7]. A cooling rate of 410 °C/s or higher leads to the complete formation of α′ martensite [16]. The cooling rate of Ti64 in the 3D printing process is around 10^3-10^5 C/s [13]. The pore can make a hole with depths up to 36 μm on the surface of the polished Ti6Al4V (Figure 4c).

3.3. X-ray diffraction pattern

The X-ray diffraction pattern (Figure 5) shows that the Ti64 printed material mainly consists of the α or α' phase. The X-ray diffraction method finds it difficult to distinguish between these phases, as both share the same hexagonal close-packed (HCP) crystal structure. The presence of the α' phase is mainly confirmed through the needle-like morphology observed in microstructural images (Figure 4b). The β phase is nearly absent in the diffraction pattern, likely due to its low content in the printed sample.

3.4. Mechanical properties

The HV hardness values and HRC equivalent hardness values at three positions of the printed sample are shown in Table 3. The average hardness of the 3D-printed Ti64 alloy sample was 343 HV. This hardness value is moderate (not excessively high), but not low either due to the coexistence of the high-hardness α' phase and the presence of large pores, which can negatively impact mechanical strength.

Table 3. *Hardness values at 3 positions on the surface of the sample*

Position	HV	HRC
Position 1	346	35.1
Position 2	332	33.5
Position 3	350	35.5
Average	343	34.7

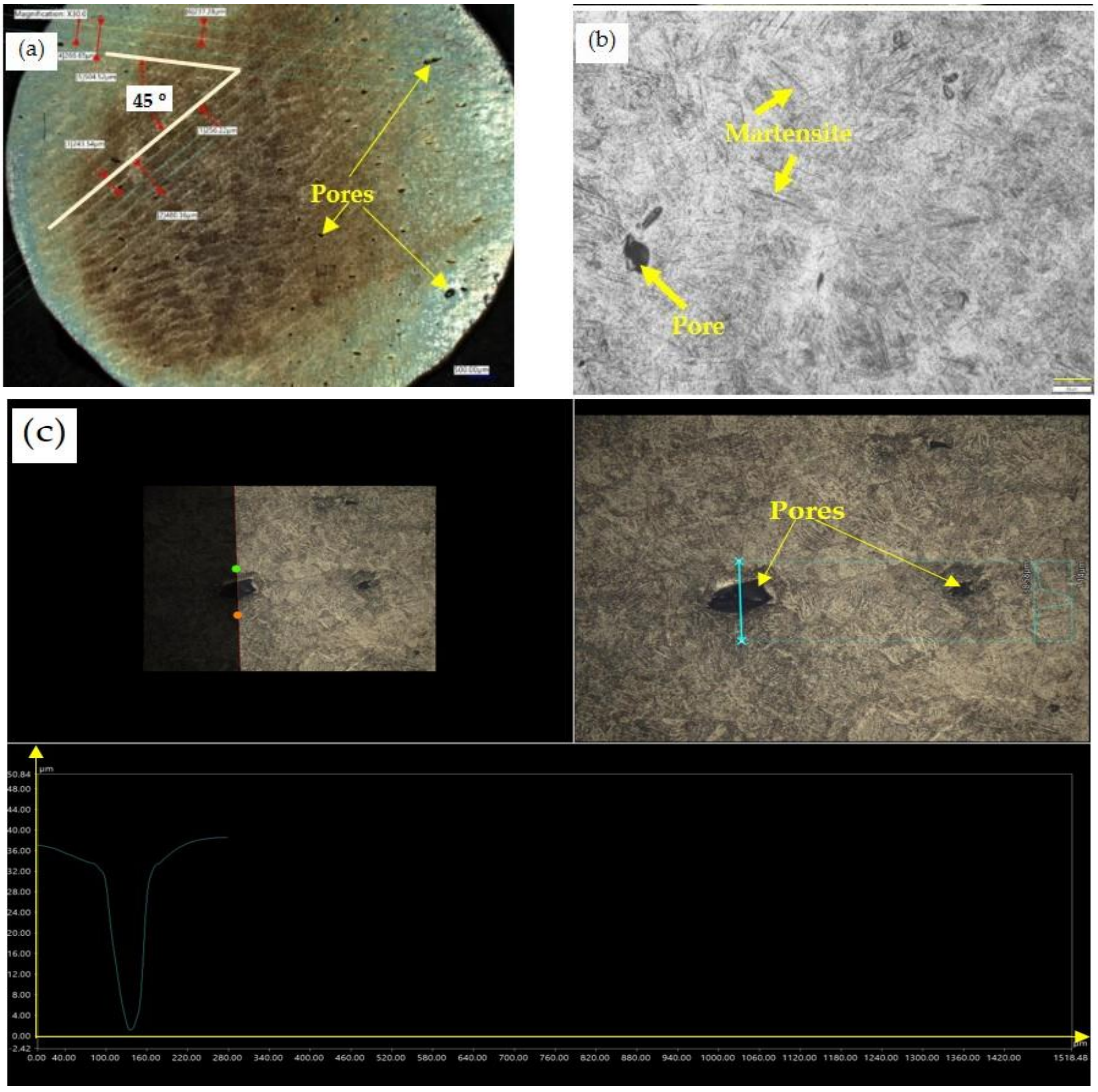

Figure 4. *Microstructure of the printed sample: a) photographed by digital microscope, b) photographed by optical microscope, and c) pore analysis by digital microscope*

The tensile test curve and fracture surface images of the tensile test specimen are presented in Figure 6 and Figure 7, respectively. From the tensile curve (Figure 6), the mechanical properties (Table 4) show that the sample exhibits low stiffness, as reflected by its low elastic modulus (E). The yield limit ($\sigma_{0.2}$) is low, causing the sample to quickly enter the plastic deformation stage. This behavior is attributed to the presence of defects, such as pores, which are observed in the microstructure (Figure 4).

Despite this, the sample demonstrates a relatively high ultimate tensile strength (σ_u), which can be explained by the formation of small, fine α/α' phases during the rapid cooling process inherent to Selective Laser Melting (SLM) technology. The ductility (δ) of the printed sample is moderate compared to conventionally manufactured Ti64. The fine-grained structure of the α/α' phases and the printed strip boundaries increases resistance to dislocation movement, enhancing strength but also reducing ductility.

Observing the fracture surface (Figure 7a and 7b), numerous dimples and voids are visible, which are characteristic of plastic deformation before failure. Additionally, fractures along grain boundaries and cleavage facets are present, indicating that brittle failure also occurred. This

suggests that the fracture behavior of the 3D-printed sample involves a combination of both ductile and brittle failure mechanisms.

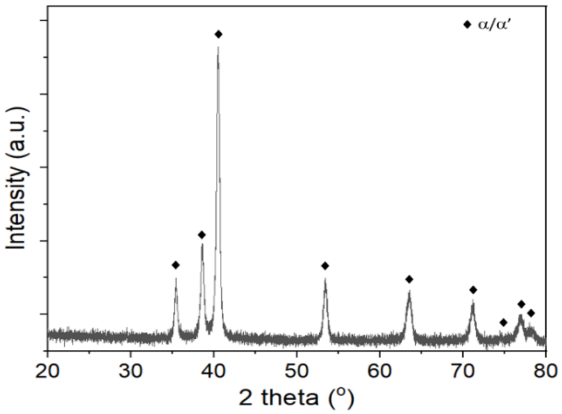

Figure 5. *X-ray diffraction pattern of the 3D-printed Ti64 sample*

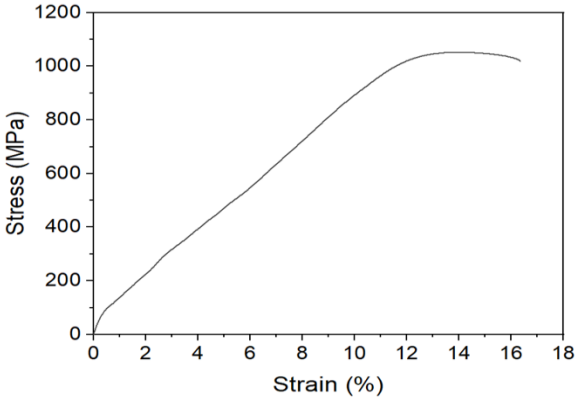

Figure 6. *Tensile curve of the 3D-printed Ti64 sample*

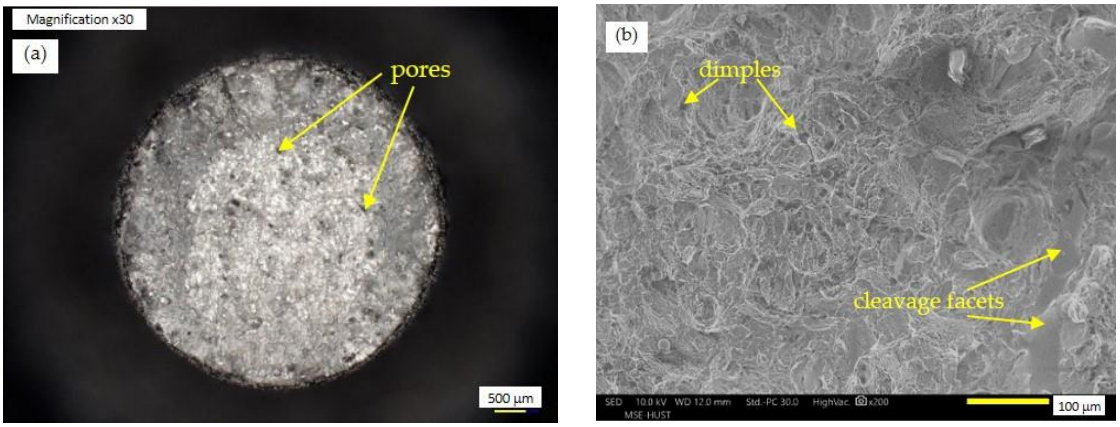

Figure 7. *Fracture surface images captured by a) digital microscope and b) scanning electron microscope*

Table 4. *Mechanical properties of the 3D-printed sample*

	E, GPa	$\sigma_{0.2}$, MPa	σ_u, MPa	δ, %
3D-printed Ti64 sample in this study	28.34	93.5	1049.4	12.8
3D-printed Ti64 sample by Electron beam based powder bed fusion (PBF) [12]	-	740±10	790±10	2.2±0.3
3D-printed Ti64 sample by Laser based powder bed fusion (PBF) [17]	-	664÷802	1040÷1062	~11.9
Conventional Ti64 sample [1]	105	948	994	21

4. Conclusion

Ti-6Al-4V (Ti64) alloy sample was fabricated using Selective Laser Melting technology and was investigated by some analysis methods. The key findings are summarized as follows:

- The 3D-printed sample exhibited an anisotropic microstructure with scan lines oriented at 45° between layers. A high surface roughness (average Ra of 72.87 µm) was observed, primarily due to unmelted powder particles. Significant porous defects were present, with pores up to 36 µm deep on polished surfaces. The microstructure mainly consisted of the α or α' phases, with the formation of needle-like α' martensite. Mechanical properties included an average hardness of 343 HV, an elastic modulus of 24.34 GPa, a yield strength of 93.5 MPa, an ultimate tensile strength of 1049.4 MPa, and a ductility of 12.8%.

- The presence of significant defects (porosity, roughness) and the consequently inferior mechanical properties compared to conventional material.

- The study was conducted using only one specific set of SLM parameters, which resulted in the observed significant porosity and high surface roughness. Future research should aim to optimize SLM process parameters to minimize defects like porosity and improve surface quality. Investigating the effects of various post-print treatments such as heat treatment on the microstructure and mechanical properties is crucial.

Acknowledgement

This research is funded by the Ministry of Education and Training (MOET) under project number B2024.BKA.15.

REFERENCES

[1] M. Motyka, K. Kubiak, J. Sieniawski, and W. Ziaja, "Phase transformations and characterization of α + β Titanium Alloys," *Comprehensive Materials Processing*, vol. 2, pp. 7–36, 2014.

[2] W. Rae, "Thermo-metallo-mechanical modelling of heat treatment induced residual stress in Ti–6Al–4V alloy," *Materials Science and Technology*, vol. 35, no. 7, pp.747–766, 2019.

[3] R. Pederson, "Microstructure and phase transformation of Ti-6Al-4V," PhD. Thesis, Luleå University of Technology, Luleå, 2002.

[4] R. Ben, F. Schöffer, G. Brian, B. Redwood, F. Schöffer, and B. Garret, *The 3D printing handbook_ technologies, design and applications*, 3D Hubs, 2017.

[5] X. Yang, R. A. Barrett, M. Tong, N. M. Harrison, and S. B. Leen, "Towards a process-structure model for Ti-6Al-4V during additive manufacturing," *J. Manuf. Process.*, vol. 61, pp. 428–439, 2021.

[6] S. Liu and Y.C. Shin, "Additive manufacturing of Ti6Al4V alloy: A review," *Materials and Design*, vol. 164, 2019, Art. no. 107552.

[7] B. Dutta and F. H. Froes, *Additive manufacturing of titanium alloys: state of the art, challenges and opportunities*, Elsevier Science, 2016.

[8] H. D. Nguyen, A. Pramanik, A. K. Basak, Y. Dong, C. Prakash, S. Debnath, S. Shankar, I. S. Jawahir, S. Dixit, and D. Buddhi, "A critical review on additive manufacturing of Ti-6Al-4V alloy: microstructure and mechanical properties," *J. Mater. Res. Technol.*, vol. 18, pp. 4641–4661, 2022.

[9] S. A. Shalnova, G. A. Panova, and N. Buczak, "Structure and phase composition of Ti-6Al-4V samples produced by direct laser deposition," *Key Eng. Mater.*, vol. 822, pp. 467–472, 2019.

[10] H. L. Wei, Y. Cao, W.H. Liao, and T. T. Liu, "Mechanisms on inter-track void formation and phase transformation during laser powder bed fusion of Ti-6Al-4V," *Additive Manufacturing*, vol. 34, 2020, Art. no. 101221.

[11] M. T. Nguyen and V. T. Trinh, "Heat treatment for microstructure stabilizing of biomedical Ti-6Al-4V alloy fabricated by selective laser melting," *MM Science Journal*, pp. 7453-7457, 2024, doi: 10.17973/MMSJ.2024_10_2024060.

[12] M. Koike, P. Greer, K. Owen, G. Lilly, L. E. Murr, S. M. Gaytan, *et al.*, "Evaluation of titanium alloys fabricated using rapid prototyping technologies—electron beam melting and laser beam melting," *Materials*, vol. 4, pp. 1776-1792, 2011.

[13] S. Al-Bermani, M. Blackmore, W. Zhang, and I. Todd, "The origin of microstructural diversity, texture, and mechanical properties in electron beam melted Ti6Al4V," *Metall. Mater. Trans. A*, vol. 41, pp. 3422–3434, 2010.

[14] G. Kasperovich and J. Hausmann, "Improvement of fatigue resistance and ductility of TiAl6V4 processed by selective laser melting," *J. Mater. Process. Technol.*, vol. 220, pp. 202–214, 2015.

[15] F. Bartolomeu, M. Gasik, F. S. Silva, and G. Miranda, "Mechanical properties of Ti6Al4V fabricated by laser powder bed fusion: A review focused on the processing and microstructural parameters influence on the final properties," *Metals*, Vol. 12, 2022, doi: 10.3390/met12060986.

[16] A. T. Ahmed and H. J. Rack, "Phase transformations during cooling in α+β titanium alloys," *Mater. Sci. Eng. A*, vol. 243, no. 1, pp. 206–211, 1998.

[17] G. Kasperovich and J. Hausmann, "Improvement of fatigue resistance and ductility of Ti-6Al-4V processed by selective laser melting," *J. Mater. Process. Technol.*, vol. 220, pp. 202–214, 2015.